ChemCatChem

The European Society Journal for Catalysis

Chemistry Europe

European Chemical Societies Publishing

Supported by GECATS GERMAN CATALYSIS SOCIETY

# Accepted Article

**Title:** CeO2@N/C@TiO2 Core-shell Nanosphere Catalyst for the Aerobic Oxidation of 5-Hydroxymethylfurfural to 5-Hydroxymethyl-2-Furancarboxylic Acid

**Authors:** yong song, Geoffrey I.N. Waterhouse, Feng Han, Yan Li, and Shiyun Ai



**To be cited as:** *ChemCatChem* 10.1002/cctc.202100091

**Link to VoR:** https://doi.org/10.1002/cctc.202100091

WILEY-VCH

 10.1002/cctc.202100091

# $CeO_2$@N/C@$TiO_2$ Core-shell Nanosphere Catalyst for the Aerobic Oxidation of 5-Hydroxymethylfurfural to 5-Hydroxymethyl-2-Furancarboxylic Acid

Yong Song[a], Geoffrey I.N. Waterhouse[b], Feng Han[a], Yan Li*[a], and Shiyun Ai*[a]

**[a] Yong Song, Prof. Dr. Feng Han, Prof. Dr. Yan Li and Prof. Dr. Shiyun Ai**

College of Chemistry and Material Science, Shandong Agricultural University, Taian, Shandong, 271018, China

Email: ashy@sdau.edu.cn

Email: liyan2010@sdau.edu.cn

**[b] Prof. Dr. Geoffrey I.N. Waterhouse**

School of Chemical Sciences, The University of Auckland Private Bag 92019, Auckland, New Zealand

## ABSTRACT

Defective D-$CeO_2$@N/C@$TiO_2$ nanospheres, each comprising a spherical $CeO_2$ core coated with shells of N-doped carbon and $TiO_2$, were successfully synthesized then evaluated for the aerobic oxidation of 5-hydroxymethylfurfural (HMF) to 5-hydroxymethyl-2-furancarboxylic acid (HMFCA). Detailed catalyst characterization studies using XRD, SEM, TEM, TG-DTA, XPS, $N_2$ physisorption confirmed the hierarchical core-shell structure of the D-$CeO_2$@N/C@$TiO_2$ nanospheres, with the defective surface structures created through a thermal hydrogenation process using $NaBH_4$ promoting HMF conversion. The effect of various reaction parameters, including the reaction time, temperature, oxygen pressure, type of alkali co-reactant and the amount of catalyst, on HMF oxidation to HMFCA over the D-$CeO_2$@N/C@$TiO_2$ nanospheres were studied. Under the optimized reaction conditions (temperature 80 °C, reaction time 30 min, $O_2$ pressure 1 MPa), a high HMF conversion of 87.8% and a remarkable HMFCA selectivity of 100% were obtained. In addition, the D-$CeO_2$@N/C@$TiO_2$ nanosphere catalyst showed great stability over four consecutive HMF oxidation tests, implying good catalyst stability. Experimental findings were used to develop a plausible reaction mechanism for the selective oxidation of HMF on the D-$CeO_2$@N/C@$TiO_2$ nanospheres.

10.1002/cctc.202100091

# INTRODUCTION

Dwindling fossil fuel reserves and escalating global energy consumption, coupled the need to curb anthropogenic $CO_2$ emissions, motivates the development of renewable energy technologies and the search for alternative fuels.[1] Biomass resources represent promising alternative to fossil fuels, both as an energy source and as a feedstock for the manufacture of important commodity chemicals.[2] Particularly important in this regard are catalytic technologies which can create valuable chemicals from simple biomass-derived platform chemicals such as 5-hydroxymethylfurfural (HMF).

Sugars in the form of monosaccharides and disaccharides can readily be obtained from biomass sources via enzymatic hydrolysis.[3] 5-Hydroxymethylfurfural, an extremely versatile platform molecule, is obtained by dehydration of glucose or fructose.[4] HMF can then be transformed into a variety of high value chemicals and fuels,[5] with some of the important oxidation products of HMF including 2,5-diformethylfuran (DFF), 5-hydroxymethyl-2-furancarboxylic acid (HMFCA), 5-formyl-2-furancarboxylic acid (FFCA), and 2,5-furandicarboxylic acid (FDCA) **(Scheme 1)**.[6] Amongst these products, FDCA and HMFCA are considered to be prized targets owing to their potential use as monomers in the synthesis of bio-based polymers.[7] HMFCA is formed by the selective oxidation of the aldehyde group in HMF, and represents a novel monomer for the synthesis of polyesters.[8] Further, HMFCA displays antitumor activity[9] and is an intermediate in the synthesis of a promising interleukin inhibitor.[10]

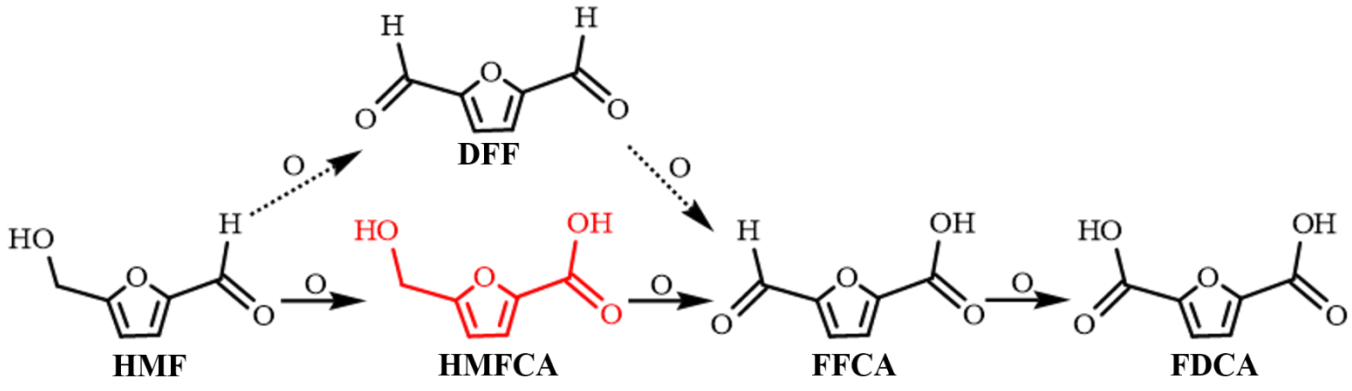


**Scheme 1. Pathways and products for the selective oxidation of 5-hydroxymethylfurfural (HMF).**

However, HMFCA is an intermediate product in the selective oxidation of HMF, and undergoes further oxidation to FDCA. As such, is often difficult to obtain HMFCA with a high selectivity

10.1002/cctc.202100091

during HMF oxidation. Synthetic methods for the selective oxidation of HMF to HMFCA are urgently needed. To date, a variety of chemical approaches, mainly based on the use of noble metal catalysts, have been explored for converting HMF into HMFCA.[8b, 11] For example, Gorbanev *et al*. evaluated the performance of an Au/$TiO_2$ catalyst for the oxidation of HMF.[5] They found that low $O_2$ pressures or low concentrations of base favored the intermediate oxidation product HMFCA relative to FDCA. Davis *et al.* prepared Au/C and Au/$TiO_2$ catalysts for the oxidation of HMF,[8a] obtaining a 92% selectivity to HMFCA with 100% conversion of HMF. Wang [12] *et al*. applied a Ru/CsPW catalyst for the oxidation of HMF, obtaining a HMF conversion of 97.2% with a HMFCA yield of 72.9%. Zhao [13] *et al.* used commercially available $Ag_2O$ as a catalyst, obtaining a HMFCA yield of 98% (60 min, 90 °C). These works demonstrate that various noble metal catalysts (Ru, Au and Ag) show good initial selectivity for the oxidation of HMF to HMFCA.[14] However, these noble metal-based catalysts have a number of drawbacks, including the high cost of the noble metals and poor recycling performance,[15] motivating the search for non-precious metal catalysts for this reaction.

To date, a few studies have been reported examining the selective oxidation of HMF to HMFCA over non-noble metal catalysts, though the studies reported show excellent promise. Zhang et al. prepared a heterogeneous catalyst (K-10 clay-Mo) for the oxidation of HMF, obtaining a HMF conversion of 100% with a HMFCA yield of 86.9% over 3 h in toluene. [16] Using a heterogeneous triazolium pre-catalyst, iron(II) phthalocyanine and air, Brandolese et al. obtained HMFCA yield of 87%. [10a] However, these reports have limitations, as they require complex organic compounds for the catalyst synthesis and use organic solvents for HMF oxidation tests. Maria Ventura et al. reported that $CeO_2$ [17], $MgO{\cdot}CeO_2$ [18]and mixed oxide systems based on cerium[19] offer good catalytic activity for the oxidation of HMF. However, the main products are FDCA and DFF, thus preventing the isolation of HMFCA as a stable intermediate. Highly selective, inexpensive and stable catalysts must be found for the direct synthesis of HMFCA.

In this work, we report the successful design of a novel core-shell structured $CeO_2$@N/C@$TiO_2$ nanosphere catalyst. The catalyst was mixed with $NaBH_4$ and heated to prepare a D-$CeO_2$@N/C@$TiO_2$ catalyst with a defective surface structure **(Scheme2)**, which offered outstanding performance for the selective catalytic oxidation of HMF to HMFCA. The oxidation of HMF tests were carried out in a sodium tetraborate solution (pH 9.18) at 80 °C and 1 MPa $O_2$, resulting in a HMF

10.1002/cctc.202100091

conversion of 89% and HMFCA selectivity of 100% after only 30 min. Catalyst recycling tests showed that the catalyst retained excellent catalytic performance after four cycles, with supporting catalysts characterization studies used to pinpoint the origins of the excellent catalytic performance.

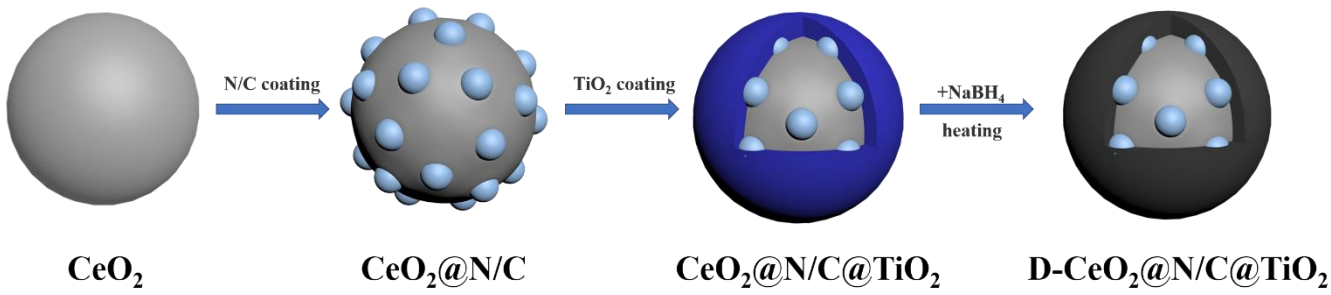


**Scheme 2. Procedure used to synthesize the D-$CeO_2$@N/C@$TiO_2$ catalyst for the selective oxidation of HMF to HMFCA.**

## MATERIALS AND METHODS

**Materials.** Cerous nitrate hexahydrate ($Ce(NO_3)_2 \cdot 6H_2O$, >98%) was purchased from Shanghai Dibo Biotechnology Co. Ltd. Potassium bromide (KBr) and tetrabutyl titanate (TBOT) were obtained from BASF Chemical Trading Co. Ltd. (TianJin, China). L-asparagine and dopamine hydrochloride were purchased from Shanghai Alighting Reagent Co. Ltd. Sodium borohydride ($NaBH_4$) was purchased from Macklin Chemical Reagent Co. Ltd. Sodium tetraborate ($Na_2B_4O_7$) buffer solution was purchased from Shanghai Hongbei Reagent Co. Ltd. Distilled deionized water was used in the experiments. Oxygen gas (99.9%) was obtained from Shandong Yingchun Gas Co. LTD.

**Preparation of $CeO_2$ nanospheres.** The $CeO_2$ nanospheres were synthesized using a hydrothermal method. Briefly, 0.585 g of $Ce(NO_3)_3 \cdot 6H_2O$, 2.252 g of KBr and 0.6 g of L-asparagine were dissolved in 50 mL of deionized water, then stirred for 1 h at room temperature. The resulting solution was then transferred to a Teflon-lined stainless-steel autoclave (volume 100 mL) and heated at 140 °C for 24 h. The $CeO_2$ nanospheres product was collected by vacuum filtration and washed successively with deionized water and ethanol (each 5 times), after which the nanospheres were dried at 70 °C for 24 h.

**Preparation of $TiO_2$ nanospheres.**

2 mL of tetrabutyl titanate and 60 mL of anhydrous acetone were mixed and stirred for 30 min at room temperature. The resulting mixture

10.1002/cctc.202100091

was then transferred to the 100 mL hydrothermal reactor. The hydrothermal reactor was then placed in an oven at 120 °C for 24 h. The $TiO_2$ nanospheres were collected by filtration, washed with deionized water 5 times, then dried at 80 °C for 12 h.

## Preparation of $CeO_2$@N/C and $TiO_2$@N/C.

For the synthesis of $CeO_2$@N/C, 20 mL of an aqueous 0.1 M tris(hydroxymethyl)aminomethane (TRIS) solution was mixed with 8 mL of an aqueous 0.1 M hydrochloric acid solution. The resulting solution then diluted to 200 mL with deionized water under continuous stirring to obtain a Tris-HCl (pH = 8.5) solution. Next, 0.5 g of the $CeO_2$ nanospheres prepared above was added to the Tris-HCl buffer solution, which was then subjected to five alternate cycles of stirring and ultrasonic treatment at room temperature (each of 30 min duration) to achieve a good $CeO_2$ nanosphere dispersion. Then, 0.03 g of dopamine hydrochloride was added, and the resulting dispersion stirred at room temperature for 24 h. The grey precipitate obtained was collected by centrifugation and washed 3 times with deionized water (300 mL each time), and subsequently dried under vacuum at 60 °C for 12 h. After drying, the sample (polydopamine coated CeO2 nanospheres, i.e. $CeO_2$@PDA) was transferred to a porcelain boat, then heated at 600 °C for 2 h under a $N_2$ atmosphere. The black product obtained was denoted herein as $CeO_2$@N/C. $TiO_2$@N/C was prepared by a similar method, except that the $CeO_2$ nanospheres were replaced by $TiO_2$ nanospheres.

## Preparation of $CeO_2$@$TiO_2$.

$CeO_2$ nanospheres (0.5 g) were ultrasonically dispersed in 100 mL of ethanol for 1 h, after which a further 50 mL of ethanol was added to the dispersion. After stirring for 30 min, tetrabutyl titanate (1.42 mL) was slowly added dropwise into the stirred dispersion. The resulting dispersion was then stirred for 12 h at room temperature, after which 10 mL of deionized water was added at a rate of 2 mL/min, with the dispersion then being stirred for a further 1 h. The solid product obtained was collected by centrifugation and washed twice with ethanol, then dried at 80 °C for 12 h. Next, the solid product was transferred to a porcelain boat and heated at 500 °C for 4 h under a $N_2$ atmosphere. The black product obtained is denoted herein as $CeO_2$@$TiO_2$.

## Preparation of $CeO_2$@N/C@$TiO_2$.

$CeO_2$@N/C (0.5 g) was ultrasonically dispersed in 100 mL of ethanol for 1 h, after which a further 50 mL ethanol was added to the dispersion. After stirring for 30 min, tetrabutyl titanate (1.42 mL)

10.1002/cctc.202100091

was slowly added dropwise into the stirred dispersion. The resulting dispersion was then stirred for 12 h at room temperature, after which 10 mL of deionized water was added at a rate of 2 mL/min, with the dispersion then being stirred for a further 1 h. The solid product obtained was collected by centrifugation and washed twice with ethanol, then dried at 80 °C for 12 h. Next, the solid product was transferred to a porcelain boat and heated at 500 °C for 4 h under a $N_2$ atmosphere. The black product was denoted herein as $CeO_2$@N/C@$TiO_2$.

**Preparation of D-$CeO_2$@N/C@$TiO_2$.** $CeO_2$@N/C@$TiO_2$ (0.5 g) and $NaBH_4$ (1 g) were mixed and ground to a homogeneous powder in a mortar and pestle. The powder blend was then heated at 500 °C for 5 h under a $N_2$ atmosphere. After the heat treatment, the product was washed 5 times with deionized water, then dried at 80 °C for 8 h. Finally, the product was ground to a fine powder, and denoted herein as D-$CeO_2$@N/C@$TiO_2$.

**Catalytic oxidation of HMF.** The catalytic oxidation of 5-HMF tests were carried out in a stainless reactor containing a 50 mL Teflon vessel. Typically, the reactor was loaded with HMF (0.1 g), $Na_2B_4O_7$ buffer solution (10 mL) and D-$CeO_2$@N/C@$TiO_2$ catalyst (0.1 g), then pressurized to 1 MPa with oxygen. The oxidation reaction was carried out at 80 °C for 0.5 h using a stirring speed of 500 rpm.

**Product Analysis.** The products formed in the catalytic oxidation of HMF tests were analyzed using a high-performance liquid chromatograph (Shimadzu, Tokyo, Japan) equipped with an ultraviolet-visible detector. Product separations were achieved on a C-18 column (Diamosil, 5 μm, 4.6 mm × 200 mm) using an acetonitrile-water mixture (5:95, v/v) as the mobile phase. The injection volume was 10 μL, the column temperature 30 °C, and the mobile phase flow rate 1.0 mL/min. The appearance times of 2,5-furandicarboxylic acid (FDCA), 5-formyl-2-furancarboxylic acid (FFCA), 5-hydroxymethyl-2-furancarboxylic acid (HMFCA), 5-hydroxymethylfurfural (HMF) and 2,5-diformethylfuran (DFF) were 4.1, 4.9, 5.5, 7.0 and 8.1 min. The detected wavelength for all products was 268 nm. Regression coefficients of the linear regression equations from the standard curves for all products were greater than 0.999.

The HMF conversion (Eq. 1) and HMFCA selectivity (Eq. 2) were defined as follows:

$$\text{HMF conversion} = \frac{\text{moles of HMF converted}}{\text{moles of added HMF}} \times 100\% \quad (1)$$

10.1002/cctc.202100091

$$\text{HMFCA selectivity} = \frac{\text{moles of HMFCA}}{\text{moles of all products}} \times 100\% \quad (2)$$

# RESULTS AND DISCUSSION

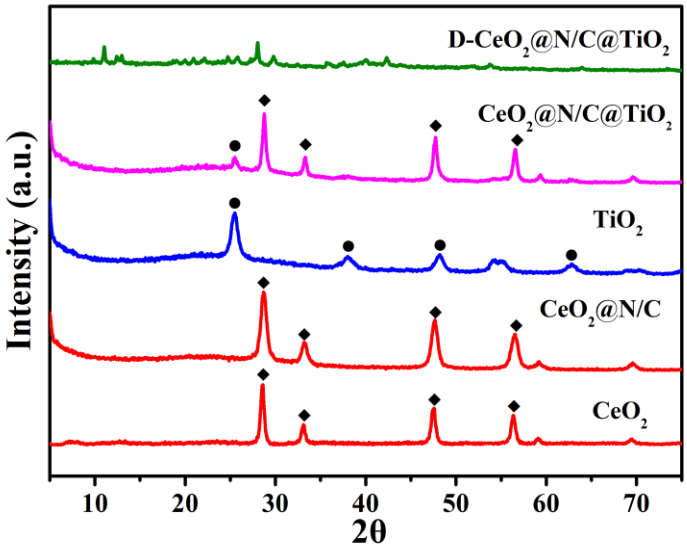


**Figure 1.** XRD patterns for $CeO_2$, $CeO_2$@N/C, $TiO_2$ and $CeO_2$@N/C@$TiO_2$.

**XRD Analysis.** XRD patterns for the $CeO_2$ nanospheres, anatase $TiO_2$, $CeO_2$@N/C and $CeO_2$@N/C@$TiO_2$, and D-$CeO_2$@N/C@$TiO_2$ are displayed in **Figure 1**. The XRD pattern for the $CeO_2$ nanospheres showed peaks at 28.54, 33.07, 47.47 and 56.33°, which could readily be assigned to the (111), (200), (220) and (311) crystal planes of cubic $CeO_2$. The XRD pattern of $CeO_2$@N/C was similar to that of the $CeO_2$ nanospheres (i.e. dominated by reflections associated with $CeO_2$). Interestingly, the $CeO_2$-related peaks were slightly broader in the $CeO_2$@N/C sample compared to the $CeO_2$ nanospheres. In addition, the $CeO_2$@N/C sample showed a very broad feature centered around 22.5 °, which we associate with an amorphous N-doped carbon shell on the $CeO_2$ nanospheres. The XRD pattern of the $CeO_2$@N/C@$TiO_2$ sample showed additional peaks due to anatase $TiO_2$, the most intense of which was the (101) reflection at 25.30°. For the D-$CeO_2$@N/C@$TiO_2$ sample, prepared by heat treatment of $CeO_2$@N/C@$TiO_2$ with $NaBH_4$, the XRD pattern contained many new and weak peaks. This indicated that the D-$CeO_2$@N/C@$TiO_2$ sample had undergone serious reduction during the mild hydrogenation treatment using $NaBH_4$, to produce $TiO_{2-x}$, $CeO_{2-x}$, $Ce(OH)_3$ and $Ce_2O_3$ and other phases.[20] This indicates that core in the $CeO_2$@N/C@$TiO_2$ was reducible, and accessible to $H_2$ generated by the

10.1002/cctc.202100091

thermal decomposition of $NaBH_4$.

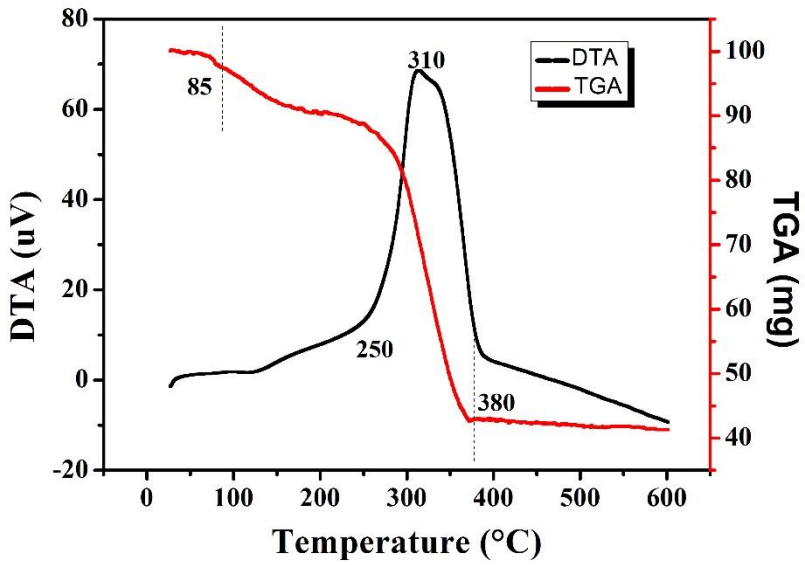


**Figure 2.** TG–DTA curves for $CeO_2$@PDA in $N_2$. The heating rate was 10 °C /min, with the analysis being performed under a $N_2$ flow.

**TG–DTA Analysis.** **Figure 2** shows TG–DTA curves for the thermal conversion of the PDA coating on the $CeO_2$ nanospheres into a N/C coating (i.e. the procedure used to form $CeO_2$@N/C). The TGA curve shows a small mass loss in the range 85-200 °C, which can be attributed to the loss of surface physisorbed water.[21] A large mass loss was observed in 250-380 °C region, which is due to the conversion of the PDA coating into a nitrogen-doped carbon (N/C coating).[22] Coinciding with this mass loss was a large exothermic peak at 310 °C in the DTA curve. Above 380 °C, no further mass loss was observed.

10.1002/cctc.202100091

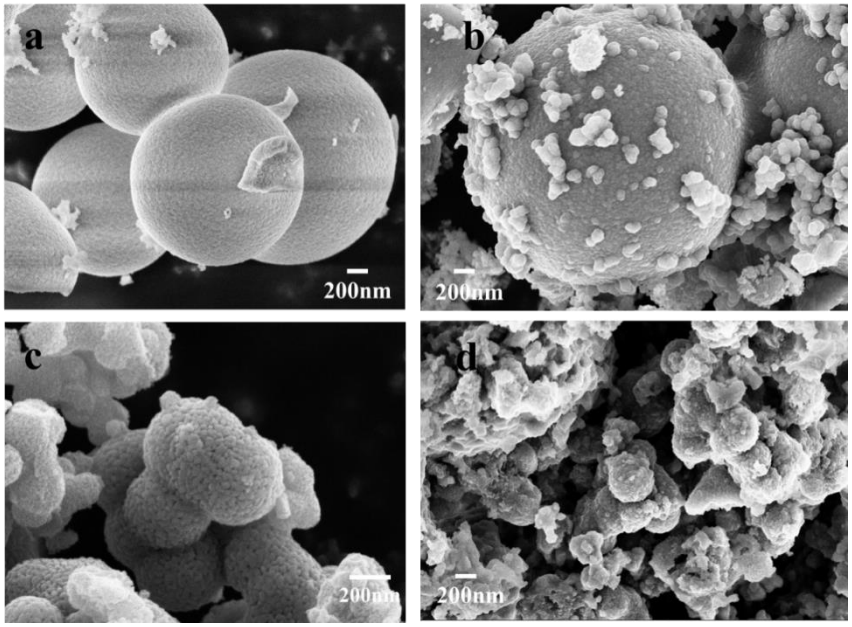


**Figure 3.** SEM images of (a) $CeO_2$, (b) $CeO_2$@N/C, (c) $CeO_2$@N/C@$TiO_2$, and (d) D-$CeO_2$@N/C@$TiO_2$.

**SEM Analysis.** The stepwise synthesis of the D-$CeO_2$@N/C@$TiO_2$ catalyst from the $CeO_2$ nanospheres, as described in Scheme 2, is capture in the SEM images of **Figure 3**. The $CeO_2$ nanospheres were spherical with diameters ranging from 1.5-2 μm (**Figure 3a).** For the $CeO_2$@N/C sample (**Figure 3b)**, many small particles can be seen coated on the surface of $CeO_2$ nanospheres, which are a N-doped carbon arising from the thermal decomposition of PDA. **Figure 3c** shows a SEM image of the $CeO_2$@N/C@$TiO_2$ specimen. The image shows that the $TiO_2$ layer formed a porous and adherent coating over the underlying $CeO_2$@N/C. After thermal reaction with $NaBH_4$, the obtained D-$CeO_2$@N/C@$TiO_2$ possessed a very rough surface and open network structure (**Figure 3d**), which likely resulted from both the surface reduction of the $TiO_2$ shell to form amorphous black $TiO_2$ ($TiO_{2-x}$) and also reduction of the $CeO_2$ core to $CeO_{2-x}$ and other Ce(III) phases. Oxygen vacancies created by the reduction treatment, associated with $Ti^{3+}$ and $Ce^{3+}$ states, were shown below to be beneficial for the selective oxidation of HMF.[23]

10.1002/cctc.202100091

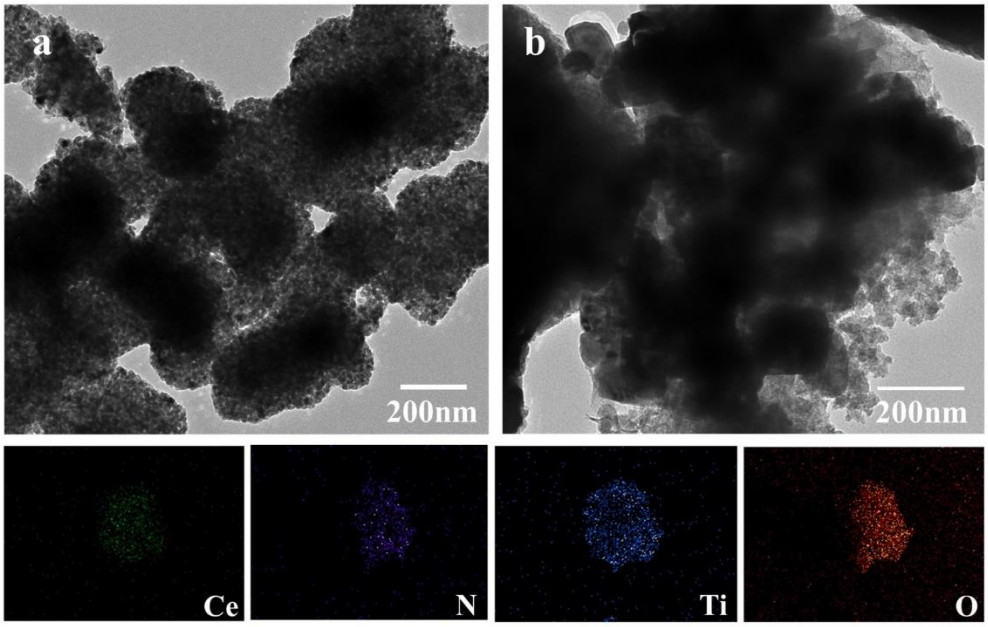


**Figure 4.** TEM images of (a) $CeO_2$@N/C@$TiO_2$ and (b) D-$CeO_2$@N/C@$TiO_2$. EDS element maps for $CeO_2$@N/C@$TiO_2$ are shown below the TEM images.

**TEM Analysis.** **Figure 4a** and **b** show TEM images for the $CeO_2$@N/C@$TiO_2$ and D-$CeO_2$@N/C@$TiO_2$ catalysts, respectively. The $CeO_2$@N/C@$TiO_2$ catalyst possessed a spherical core-shell structure, with the $TiO_2$ shell being highly porous and composed of small anatase $TiO_2$ crystallites. EDS elemental mapping images revealed a very homogeneous dispersion of Ti, O, N over the Ce-rich core. After reduction with $NaBH_4$, the D-$CeO_2$@N/C@$TiO_2$ catalyst showed a similar core-shell morphology, though the shell around the nanosphere core was more irregular, and composed of larger particles (as was also seen by SEM). Heat treatment of $TiO_2$ powders with $NaBH_4$ generally leads to the formation of an amorphous $TiO_{2-x}$ shell on the surface of the $TiO_2$ particles, which was also expected to occur here and contribute to the excellent catalytic activity of D-$CeO_2$@N/C@$TiO_2$ for HMF oxidation.

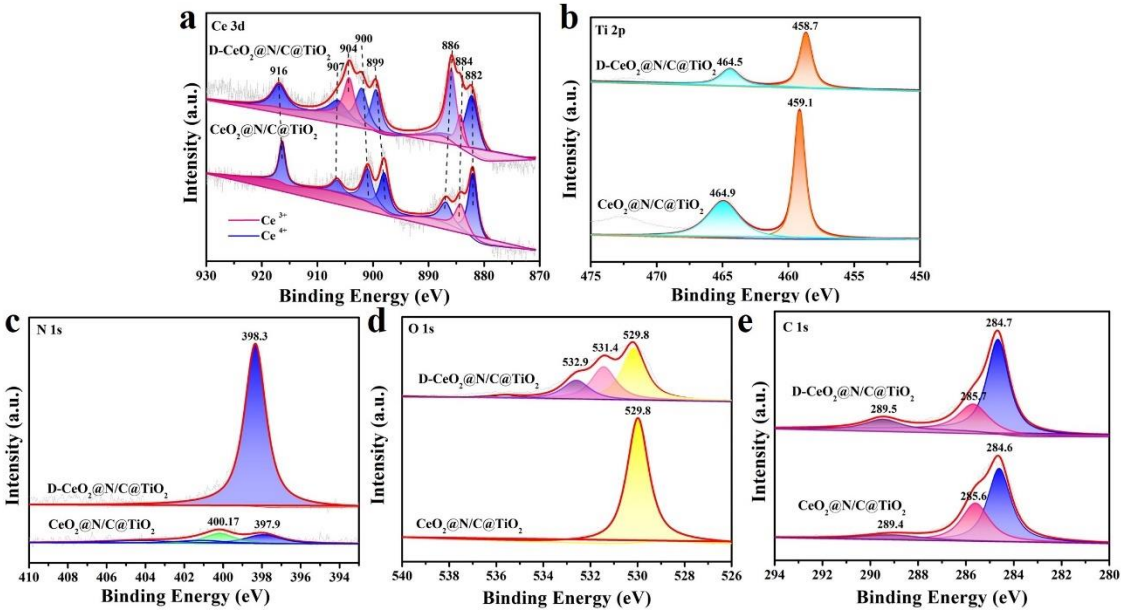


**Figure 5.** High resolution XPS spectra for $CeO_2$@N/C@$TiO_2$ and D-$CeO_2$@N/C@$TiO_2$. (a) Ce 3d region, (b) Ti 2p region, (c) N 1s region, (d) O 1s region, (e) C 1s region.

**XPS Analysis.** X-ray photoelectron was used to study the chemical changes that occurred during the reduction of $CeO_2$@N/C@$TiO_2$ to D-$CeO_2$@N/C@$TiO_2$ by thermal treatment with $NaBH_4$. **Figure 5a** shows Ce 3d XPS spectra for $CeO_2$@N/C@$TiO_2$ and D-$CeO_2$@N/C@$TiO_2$. The $CeO_2$@N/C@$TiO_2$ sample showed peaks at 882.0, 886.8, 897.9, 900.9, 906.4 and 916.3 eV typical for $Ce^{4+}$ in $CeO_2$, with weaker peaks at 884.2 and 904.3 eV being due to $Ce^{3+}$.[24] The D-$CeO_2$@N/C@$TiO_2$ sample also showed peaks for the $Ce^{4+}$ and $Ce^{3+}$ states, though the latter were more intense compared to the spectrum for the $CeO_2$@N/C@$TiO_2$ sample. For $CeO_2$@N/C@$TiO_2$, fraction of cerium present as $Ce^{3+}$ was calculated to be ~12% using the formula: Concentration ($Ce^{3+}$) = $A(Ce^{3+})/[A(Ce^{3+}) + A(Ce^{4+})]$, where $A(Ce^{3+})$ and $A(Ce^{4+})$ are peak areas for the $Ce^{3+}$ and $Ce^{4+}$ signals, respectively, in the Ce 3d spectrum.[25] For D-$CeO_2$@N/C@$TiO_2$, the concentration of $Ce^{3+}$ was higher, calculated to be ~20%. This implies that the $NaBH_4$ treatment resulted in the reduction of some $Ce^{4+}$ to $Ce^{3+}$.

The Ti 2p XPS spectrum for CeO2@N/C@TiO2 (**Figure 5b)** showed peaks at 459.1 eV and 464.9 eV in a characteristic 2:1 area ratio, which could readily be assigned to the Ti $2p_{3/2}$ and Ti $2p_{1/2}$ signals, respectively, of $Ti^{4+}$ in $TiO_2$.[26] For D-$CeO_2$@N/C@$TiO_2$, the Ti $2p_{3/2}$ and Ti $2p_{1/2}$ signals were observed at slightly lower binding energies (458.7 and 464.5 eV, respectively), implying that Ti cations in D-$CeO_2$@N/C@$TiO_2$ were of a lower

10.1002/cctc.202100091

oxidation state (presumably containing both $Ti^{4+}$ and some $Ti^{3+}$).[26a]

**Figure 5c** shows N 1s XPS spectra for $CeO_2$@N/C@$TiO_2$ and D-$CeO_2$@N/C@$TiO_2$. The spectrum for $CeO_2$@N/C@$TiO_2$ contained peaks at 397.9 and 400.1eV, which can readily be assigned to pyridinic N and pyrrolic N in the N/C shell. By comparison, the D-$CeO_2$@N/C@$TiO_2$ sample showed only a single peak at 398.3eV due to pyridinic N.[14, 24a, 27] Further, the amount of nitrogen (as pyridinic N) appeared to be greatly enhanced in the D-$CeO_2$@N/C@$TiO_2$ sample. To explain this, it needs to be remembered that XPS is a surface analytical technique, probing the top few nanometers of the sample. For $CeO_2$@N/C@$TiO_2$, the uniform $TiO_2$ coating meant that not much of the N-doped carbon shell will be probed during the experiment. For D-$CeO_2$@N/C@$TiO_2$, the $TiO_2$ shell iswas more disordered and macroporous, thus allowing more of the underlying N/C shell to be probed during the XPS analysis. Importantly, pyridinic N well-known for its oxygen activation properties, and thus was expected to be beneficial for the selective oxidation of HMF over D-$CeO_2$@N/C@$TiO_2$.

The O 1s XPS spectrum for $CeO_2$@N/C@$TiO_2$ (**Figure 5d**) showed a peak at 529.8 eV due to lattice oxygen in $TiO_2$.[28] The D-$CeO_2$@N/C@$TiO_2$ sample showed peaks at 529.8,[28] 531.4[28] and 532.9 eV [26a], which are assigned to lattice oxygen in $TiO_2$,[29] oxygen vacancies[30] and chemisorbed oxygen, respectively. The presence of the oxygen vacancies and chemisorbed oxygen were expected to enhance the catalytic performance of D-$CeO_2$@N/C@$TiO_2$ for HMF oxidation, as was confirmed by experiment below.

The C 1s XPS spectra of $CeO_2$@N/C@$TiO_2$ and D-$CeO_2$@N/C@$TiO_2$ showed peaks at 284.6, 285.7 and 289.5eV which were attributed to C-C/C=C, C-N/C=N and O-C=O groups,[31] respectively (**Figure 5e**). The presence of the C-N/C=N features in the C 1s spectra, and pyridinic N in the N 1s spectra, imply that $CeO_2$@N/C@$TiO_2$ and D-$CeO_2$@N/C@$TiO_2$ both contained N atoms doped into the graphitic carbons domains.[28]

 10.1002/cctc.202100091

**Table 1. Summarized $N_2$ physisorption data for $CeO_2$, $CeO_2$@N/C, $CeO_2$@ N/C@$TiO_2$ and D-$CeO_2$@N/C@$TiO_2$.**

| Catalyst | BET surface area ($m^2/g$) | BJH Pore diameter (Å) | BJH Pore volume ($m^3/g$) |
|---|---|---|---|
| $CeO_2$ | 0.78 | 358.9 | 0.599 |
| $CeO_2$@N/C | 35.60 | 355.4 | 0.151 |
| $CeO_2$@N/C@$TiO_2$ | 61.87 | 115.2 | 0.156 |
| D-$CeO_2$@N/C@$TiO_2$ | 40.38 | 231.2 | 0.186 |

**Surface Area and Porosity of the Different Catalysts.** $N_2$ physisorption isotherms were collected at 77 K for the $CeO_2$, $CeO_2$@N/C, $CeO_2$@N/C@$TiO_2$ and D-$CeO_2$@N/C@$TiO_2$ catalysts. BET specific surface areas, BJH pore volumes and BJH average pore diameters extracted from the physisorption data is summarized in **Table 1**. The $CeO_2$ nanospheres had a specific surface area of only 0.78 $m^2/g$. The specific surface area of spherical particles is inversely proportional to the diameter of the particles.[32] SEM characterization showed that the $CeO_2$ particles used in this work were spherical with a diameter of ~1600 nm. Accordingly, the specific surface of the spherical $CeO_2$ particles was low. A larger $CeO_2$ particle diameter was useful here for achieving a high loading and uniform distribution of N/C and $TiO_2$. The specific surface area of the nanospheres progressively increased after coating first with the N/C shell ($CeO_2$@N/C, 35.60 $m^2/g$) and then the $TiO_2$ shell ($CeO_2$@N/C@$TiO_2$, 61.87 $m^2/g$). However, the specific surface area of the D-$CeO_2$@N/C@$TiO_2$ catalyst was only 40.38 $m^2/g$, approximately 35% smaller than $CeO_2$@N/C@$TiO_2$.

ICP-OES analysis showed that the Ti and Ce contents in the D-$CeO_2$@N/C@$TiO_2$ catalyst were 24.36 wt.% and 26.94 wt.%, respectively (Table S1). This corresponds to a $CeO_2$:$TiO_2$ molar ratio of ~1:2.65. EDS mapping analyses showed the N and C contents in the D-$CeO_2$@N/C@$TiO_2$ catalyst to be 12.37 wt.% and 4.58 wt.%, respectively.

10.1002/cctc.202100091

**Table 2. Performance comparison of different catalysts for the selective oxidation of HMF.**

| Catalyst | HMF conv. (%) | Product selectivity (%) | | |
|---|---|---|---|---|
| | | HMFCA | FFCA | DFF |
| $CeO_2$ (S=67 $m^2/g$) | 49.6 | 37.3 | 62.7 | - |
| $CeO_2$ (S = 0.78 $m^2/g$) | 47.6 | 42.8 | 57.1 | - |
| $CeO_2$@N/C | 54.0 | 56.3 | 43.7 | - |
| $TiO_2$ | 35.5 | 26.8 | 73.2 | - |
| $TiO_2$@N/C | 43.2 | 43.8 | 56.1 | |
| $CeO_2$-$TiO_2$ | 61.5 | 55.8 | 44.2 | - |
| $CeO_2$@$TiO_2$ | 68.9 | 68.3 | 31.7 | |
| $CeO_2$@N/C@$TiO_2$ | 79.7 | 72.6 | 19.3 | 8.0 |
| D-$CeO_2$@N/C@$TiO_2$ | 87.8 | 100.0 | - | - |

Reaction conditions: HMF (0.1 g), $Na_2B_4O_7$ buffer solution (10 mL), catalyst (0.1 g), T = 80 °C, $P(O_2)$ = 1 MPa, reaction time = 30 min.

**Catalyst Screening.** An initial set of HMF oxygenation tests were conducted over the various catalysts at a temperature of 80 °C and an $O_2$ pressure of 1.0 MPa. The reaction time was 30 min, with the results being summarized in **Table 2**. $CeO_2$ and $TiO_2$ showed modest activities for HMF conversion, and also modest selectivities towards HMFCA. $CeO_2$ surface area had little influence on HMF oxidation activity or product selectivities. The $CeO_2$@N/C and $TiO_2$@N/C catalysts, and the mixed oxide catalysts ($CeO_2$-$TiO_2$, $CeO_2$@$TiO_2$), offered a slightly higher conversion of HMF and improved selectivity of HMFCA. Not surprisingly therefore, the $CeO_2$@N/C@$TiO_2$ catalyst offered a higher conversion of HMF (79.7%) and also improved selectivity of HMFCA (72.6%). Results suggest that the N/C coating was beneficial for the adsorption and transformation of molecular $O_2$, thus boosting HMF oxidation to HMFCA. The D-$CeO_2$@N/C@$TiO_2$ showed the highest conversion of HMF (87.8%), with a remarkable selectivity to HMFCA of 100%. Clearly, chemical and structural changes introduced during $CeO_2$@N/C@$TiO_2$

10.1002/cctc.202100091

heating with $NaBH_4$ contributed enormously to the improved catalytic properties of D-$CeO_2$@N/C@$TiO_2$.

We calculated the C, H, O mass balance when $CeO_2$, $CeO_2$@N/C, $CeO_2$@$TiO_2$, $CeO_2$@N/C@$TiO_2$ and D-$CeO_2$@N/C@$TiO_2$ were used as catalysts. As shown in Table S2, the total molar amount of HMF (unreacted + converted) was approximately equal to the molar amount of HMF used in the tests, indicating negligible amounts of HMF remained adsorbed on the catalysts (thus the HMF conversions reported here were not exaggerated simply by reactant adsorption on the catalysts).

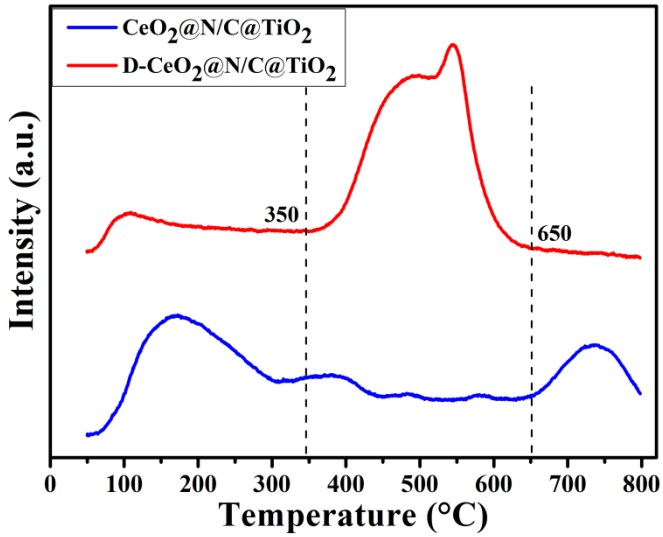


**Figure 6**. $O_2$-TPD curves for $CeO_2$@N/C@$TiO_2$ and D-$CeO_2$@N/C@$TiO_2$

**$O_2$-TPD Analysis.** Since the oxidation of HMF to HMFCA requires $O_2$ adsorption and activation, $O_2$-TPD curves were collected for $CeO_2$@N/C@$TiO_2$ and D-$CeO_2$@N/C@$TiO_2$ (**Figure 6**). Oxygen desorption signals in the range of 50-350 °C can generally be ascribed to weakly bound molecular physisorbed and/or chemisorbed oxygen ($O_2^-$, $O^-$),[33] sometimes termed α-O species. Desorption peaks in the range of 350-650 °C are due to the release of lattice oxygen ($O_{latt}$, $O^{2-}$) as $O_2$,[33a] and are termed β-O species. At temperatures higher than 650 °C, γ-O species may be seen resulting from the migration of lattice oxygen in the structure of the catalyst[34]. $CeO_2$@N/C@$TiO_2$ showed peaks due α-O and γ-O species, along with some weak β-O features. Conversely, D-$CeO_2$@N/C@$TiO_2$ showed predominantly β-O species. [35] This may be due to the fact that D-$CeO_2$@N/C@$TiO_2$ was rich in surface defects such

10.1002/cctc.202100091

as oxygen vacancies, resulting in very strong binding of molecular oxygen and/or good oxygen storage ability (e.g. $CeO_{2-x} + x/2O_2 \leftrightarrow CeO_2$).

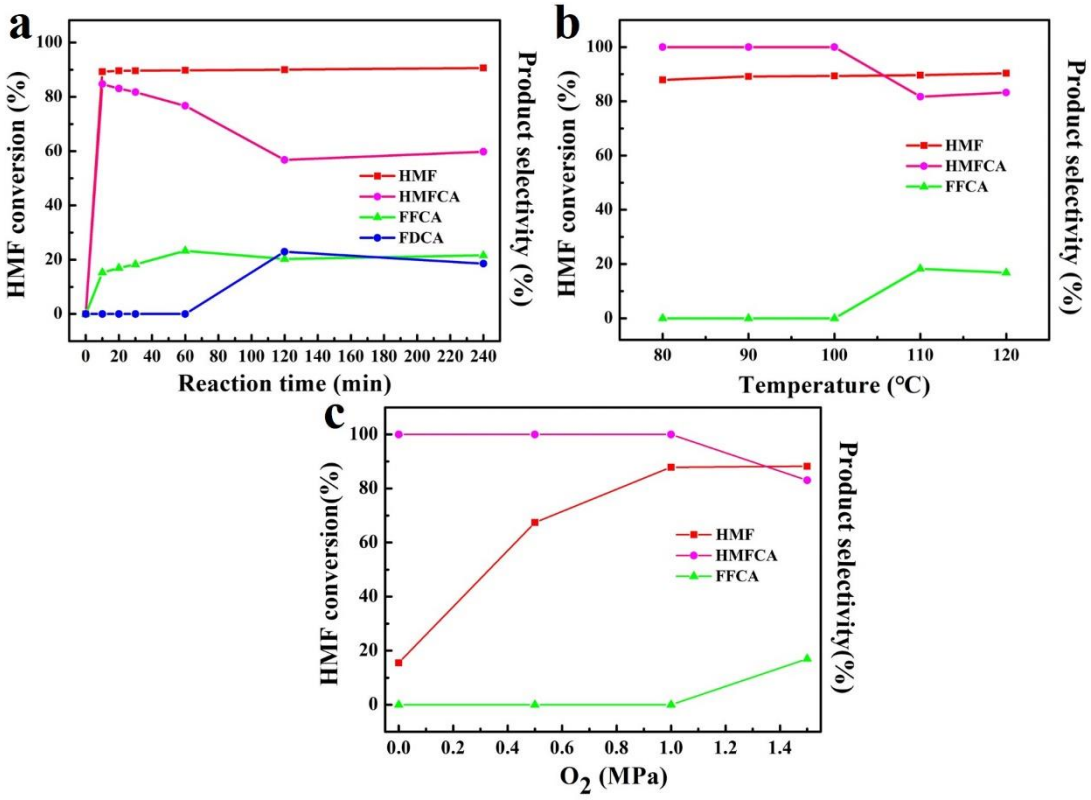


**Figure 7.** Effect of (a) reaction time, (b) temperature and (c) $O_2$ pressure on the selective oxidation of HMF over D-$CeO_2$@N/C@$TiO_2$. Reaction conditions: (a) 0.1 g catalyst, 1 MPa $O_2$, 0.1g HMF, 110 °C (b) 0.1 g catalyst, 1 MPa $O_2$, 30 min, 0.1g HMF (c) 0.1 g catalyst, 0.1g HMF, 30 min, 80 °C.

**Effect of Reaction Time, Temperature and $O_2$ Pressure on HMF Oxidation.** In order to determine the optimal conditions for the catalytic oxidation of HMF to HMFCA over D-$CeO_2$@N/C@$TiO_2$, the effects of reaction time, reaction temperature and oxygen pressure were investigated in detail. **Figure 7a** shows the effect of reaction time on the oxidation of HMF. The conversion of HMF reached ~89.2% after 10 min and then remained relatively constant as the reaction time was increased to 4 h. As the reaction time increased, the selectivity to FFCA and FDCA progressively increased, as expected based on Scheme 1. A reaction time of 30 min thus afforded the highest HMFCA yield, and was used in subsequent experiments.

10.1002/cctc.202100091

**Figure 7b** shows the effect of reaction temperature on the oxidation of HMF. It can be seen that the conversion of HMF slightly increased with temperature in the range 80-120 °C, reaching 90.3% at 120 °C. The selectivity of HMFCA was ~100% in the temperature range of 80-100 °C, but decreased at temperatures above 100 °C due to FFCA formation. Hence, a temperature of 80 °Cwas used in the subsequent experiments.

**Figure 7c** shows the effect of $O_2$ pressure on the oxidation of HMF. It can be seen that in the absence of oxygen, the conversion of HMF was only 15.5% with a selectivity to HMFCA of 100%. When the $O_2$ pressure was increased to 1 MPa, the conversion of HMF increased to 87.8% with no change in the selectivity to HMFCA (still 100%). However, on raising the pressure of $O_2$ to 1.5 MPa, the selectivity to HMFCA decreasesd to 83% due to the formation of FFCA. Accordingly, 1 MPa of $O_2$ was identified as the optimal oxygen gas pressure for the selective oxidation of HMF to HMFCA over the D-$CeO_2$@N/C@$TiO_2$ catalyst (at a reaction time of 30 min and a reaction temperature of 80 °C).

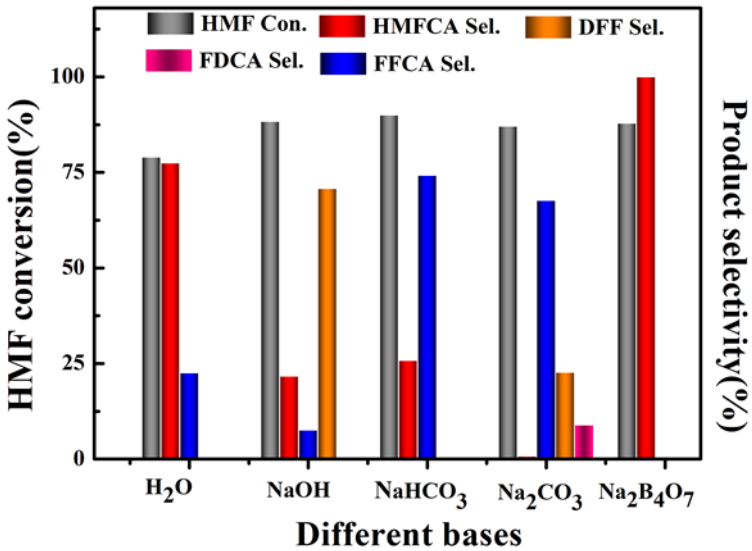


**Figure 8.** Effect of different bases on the HMF selective oxidation performance of D-$CeO_2$@N/C@$TiO_2$. Reaction conditions: 0.1 g catalyst, 1 MPa $O_2$, 0.1g HMF, 80 °C, 30 min. The molar ratio of the added base amount to HMF was 1:1 in all experiments.

**Effect of Different Bases on HMF Oxidation.** In a previous work, Zhao et al. studied the effect of different bases on the catalytic oxidation of HMF,[13] with both HMF conversion and product selectivities depending on the base

10.1002/cctc.202100091

used. Accordingly, we explored the effect of different alkali solutions on the catalytic oxidation of HMF by D-$CeO_2$@N/C@$TiO_2$. As shown in the **Figure 8**, the conversion of HMF in water was 78%, with a HMFCA selectivity of 77%. We then examined the influence of the different alkali additives (NaOH, $Na_2CO_3$, $NaHCO_3$, $Na_2B_4O_7$) at a 1:1 ratio to HMF. The pH of the reaction solutions were 12.73, 11.47, 8.45, and 9.18, respectively. As shown in Figure 8, when the pH of the catalytic reaction is high, the selectivity to DFF increased.[36] When the pH is low, the selectivity to HMFCA was variable. When the pH of the reaction solution was weakly alkaline, as in the case of aqueous $Na_2B_4O_7$ (pH = 9.18), the selectivity to HMFCA was optimized (~ 100%).

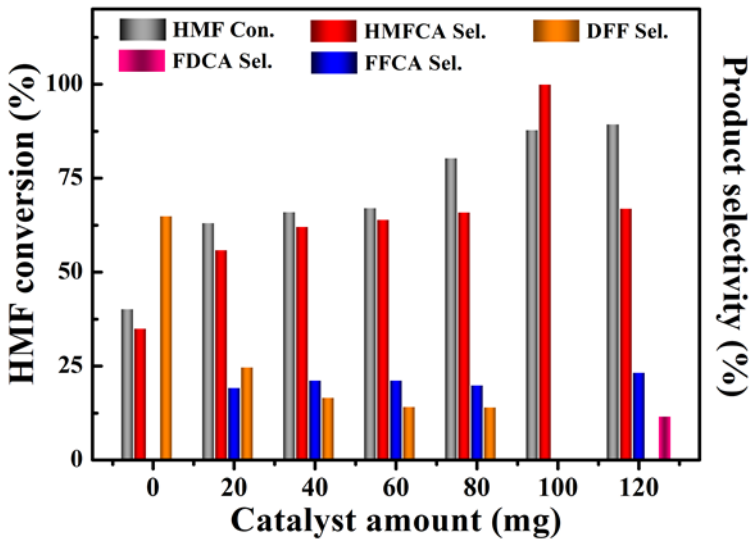


**Figure 9.** Effect of catalyst amount on the HMF selective oxidation performance of D-$CeO_2$@N/C@$TiO_2$. Reaction conditions: 1 MPa $O_2$, 0.1g HMF, 80 °C, 30 min, $Na_2B_4O_7$ buffer solution (pH 9.18).

**Effect of Catalyst amount on HMF Oxidation.** **Figure 9** shows the effect of the amount of D-$CeO_2$@N/C@$TiO_2$ catalyst on the oxidation of HMF. In the absence of catalyst, the HMF conversion was only 40% with a HMFCA selectivity of only 35%. On increasing the catalyst amount to 20 mg, the conversion of HMF and the selectivity of HMFCA both improved to 63% and 55%, respectively. On increasing the amount of catalyst further, the conversion of HMF and the selectivity to HMFCA continued to increase. When the amount of catalyst was 100 mg, the conversion of HMF and the selectivity to HMFCA were optimized at 87.8% and 100%, respectively.

10.1002/cctc.202100091

While the selectivity to DFF decreased as the amount of catalyst increased, due to DFF conversion to FFCA. The selectivity to HMFCA decreased when the catalyst amount exceeded 100 mg, thus 100 mg of the D-$CeO_2$@N/C@$TiO_2$ catalyst was identified as the optimal amount for the selective oxidation of HMF to HMFCA. When the amount of catalyst was 120 mg, peroxidation to form FDCA occurred.

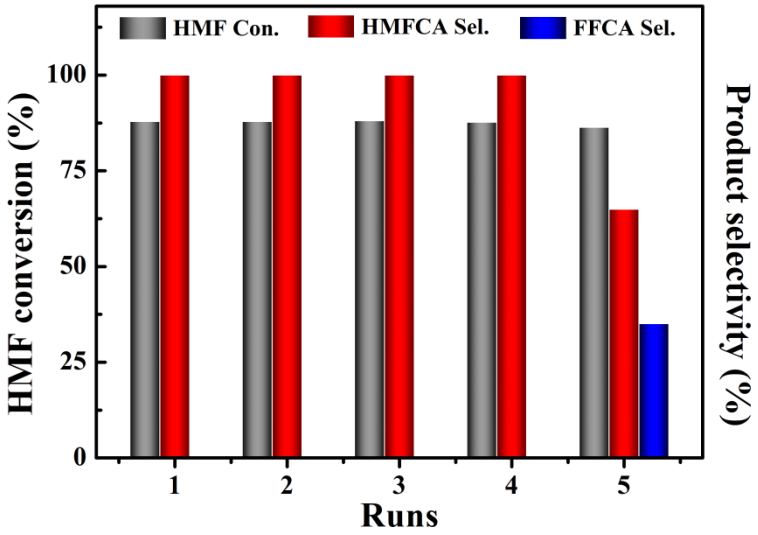


**Figure 10**. Effect of catalytic test run on the HMF selective oxidation performance of D-$CeO_2$@N/C@$TiO_2$. Reaction conditions: 1 MPa $O_2$, 0.1g HMF, 80 °C, 30 min, $Na_2B_4O_7$ buffer solution (pH 9.18).

**Catalyst Recycling Tests.** The recyclability of the D-$CeO_2$@N/C@$TiO_2$ catalyst for the selective oxidation of HMF to HMFCA was also investigated. **Figure 10** shows that D-$CeO_2$@N/C@$TiO_2$ retained outstanding performance over the first four runs, with negligible change in the conversion of HMF (~87 %) or the selectivity of HMFCA (~100 %). In the fifth cycle, the conversion of HMF decreased slightly whilst the selectivity to HMFCA decreased to 64.9%, along with a concomitant increase in the selectivity to FFCA. The reason for this sudden drop in selectivity to HMFCA needs more investigation, though is likely associated with a chemical change on the surface of the D-$CeO_2$@N/C@$TiO_2$ catalyst (such as full oxidation of the initially defective $CeO_{2-x}$ core to stoichiometric $CeO_2$).

The physicochemical and textural properties of the used catalysts were studied. XPS, $O_2$-TPD and SEM studies were performed on catalysts after 4 and 5 cycles of HMF oxidation. The results of these physicochemical and texture analyses are summarized below.

10.1002/cctc.202100091

As shown in Fig S1, as the number of cycles of HMF oxidation tests increased from 4 to 5, the amount of $Ce^{3+}$ in the catalyst increased. This may be due to electron transfer to $Ce^{4+}$ ions, or alternatively the formation of $CeO_{2-x}$ phase via loss of lattice oxygen. Evidence for this is seen in the $O_2$-TPD data (Fig S2). After 4 cycles, the catalyst had a lot of β-O, which can convert lattice oxygen into surface chemisorbed oxygen via assisting oxygen migration.[33a] After 5 cycles, the amount of β-O in the catalyst was greatly reduced. Fig S3 shows SEM images of catalysts after 4 and 5 cycles of HMF oxidation. After 4 cycles, the catalyst structure had collapsed to some extent, though still retained a porous structure. However, after 5 cycles of tests, serious agglomeration and densification of the catalyst was observed, which obviously played a key role in the decreased activity of the catalyst.

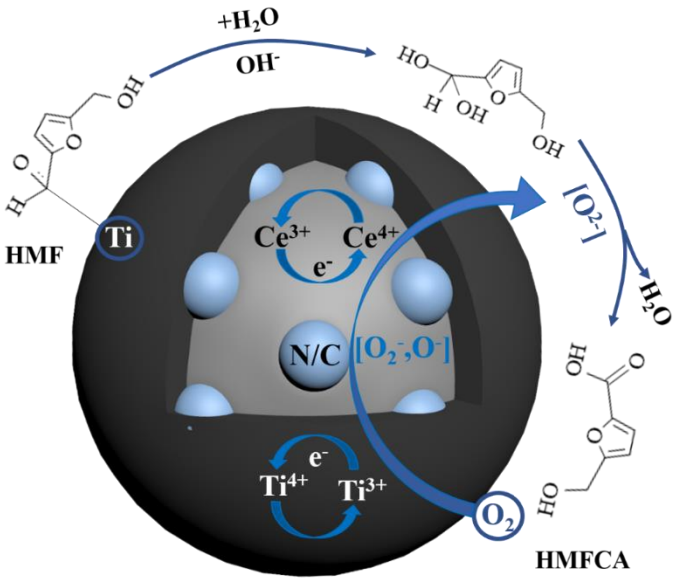


**Scheme 3. Reaction mechanism for HMF oxidation over the D-$CeO_2$@N/C@$TiO_2$ catalyst.**

**Catalytic mechanism.** Based on the above results, a plausible reaction mechanism for HMF oxidation to HMFCA on the D-$CeO_2$@N/C@$TiO_2$ catalyst was developed **(scheme 2)**. In the presence of an added base, $OH^-$ ions activate the aldehyde group of HMF, in the process generating a hemiacetal or gem diol intermediate which is subsequently dehydrogenated to form a carboxylic acid.[37] In the initial step of the reaction, the aldehyde group of HMF is first adsorbed onto the strong Lewis acid sites ($Ti^{4+}$ species) of the $TiO_2$ outer coating, then being transformed into a gem diol intermediate through a hydration reaction.[38] Meanwhile, defective $Ti^{3+}$ species created during

10.1002/cctc.202100091

the catalyst synthesis are oxidized to $Ti^{4+}$ species via the release an electron, which cause the reduction $Ce^{4+}$ in the core to $Ce^{3+}$.[39] A gaseous $O_2$ molecule then adsorbs on the N-doped carbon (i.e. N/C) component of the catalyst which is rich in pyridinic sites, resulting in chemisorbed oxygen species such as $O_2^-$ and $O^-$, with the latter becoming part of the $CeO_2$ lattice ($O^{2-}$).[37] The gem diol intermediate then undergoes oxidative dehydrogenation to HMFCA and one molecule of water.[40]

10.1002/cctc.202100091

# CONCLUSIONS

A D-$CeO_2$@N/C@$TiO_2$ catalyst with a defective surface was successfully prepared by heat treatment of a core-shell structured $CeO_2$@N/C@$TiO_2$ material with $NaBH_4$ at 500 °C in $N_2$ for 5 h. Catalytic oxidation tests conducted in a pressurized reactor demonstrated that D-$CeO_2$@N/C@$TiO_2$ possessed exceptional selectivity for the oxidation of HMF to HMFCA in the presence of $O_2$. Under optimized testing conditions (100 mg catalyst, 80 °C, 1 MPa $O_2$, reaction time 30 min, $Na_2B_4O_7$ buffer), a HMF conversion of 87.8% and a HMFCA selectivity of 100% was achieved. $O_2$-TPD revealed that the D-$CeO_2$@N/C@$TiO_2$ catalyst was very effective in converting surface adsorbed oxygen into $CeO_2$ lattice oxygen. The components of the D-$CeO_2$@N/C@$TiO_2$ catalyst, such as Lewis acid $Ti^{4+}$ sites in the outer shell for HMF adsorption, pyridinic N sites in the N/C layer for $O_2$ activation, and the mixed $Ce^{3+}$/$Ce^{4+}$ states in the $CeO_2$ core, all act synergistically to tune the activity and selectivity of the catalytic reaction. Importantly, D-$CeO_2$@N/C@$TiO_2$ showed negligible change in performance over four consecutive catalytic tests, suggesting that the developed noble-metal free catalyst has excellent promise for the synthesis of valuable HMFCA from HMF.

10.1002/cctc.202100091

## Conflicts of interest

The authors declare no competing financial interest.

## ACKNOWLEDGMENTS

This work was financially supported by the Shandong Provincial Natural Science Foundation of China (No. ZR2017MB035). GINW acknowledges funding support from the MacDiarmid Institute for Advanced Materials and Nanotechnology, and Shandong Provincial Double Hundred Talents Programme for Foreign Experts.

**KEYWORDS:** Aerobic oxidation, Core-shell nanospheres, Defective, HMF, HMFCA

# REFERENCES


[1] aA. J. Ragauskas, C. K. Williams, B. H. Davison, G. Britovsek, J. Cairney, C. A. Eckert, W. J. Frederick, Jr., J. P. Hallett, D. J. Leak, C. L. Liotta, J. R. Mielenz, R. Murphy, R. Templer, T. Tschaplinski, *Science* **2006**, *311*, 484-489; bY. Wang, B. Liu, K. Huang, Z. Zhang, *Industrial & Engineering Chemistry Research* **2014**, *53*, 1313-1319; cM. Ventura, M. Aresta , A. Dibenedetto, *ChemSusChem* **2016**, *9*, 1096-1100.

[2] aY.T. Liao, V. C. Nguyen, N. Ishiguro, A. P. Young, C.-K. Tsung, K. C. W. Wu, *Applied Catalysis B: Environmental* **2020**, *270*, 118805; bM. Ventura, D. Williamson, F. Lobefaro, M. D. Jones, D. Mattia, F. Nocito, M. Aresta, A. Dibenedetto, *ChemSusChem* **2018**, *11*, 1073-1081.

[3] aT. Schafer, T. W. Borchert, V. S. Nielsen, P. Skagerlind, K. Gibson, K. Wenger, F. Hatzack, L. D. Nilsson, S. Salmon, S. Pedersen, H. P. Heldt-Hansen, P. B. Poulsen, H. Lund, K. M. Oxenboll, G. F. Wu, H. H. Pedersen, H. Xu, *Advances in biochemical engineering/biotechnology* **2007**, *105*, 59-131; bY. Y. Gorbanev, S. K. Klitgaard, J. M. Woodley, C. H. Christensen, A. Riisager, *ChemSusChem* **2009**, *2*, 672-675.

[4] aZ. Miao, Y. Zhang, X. Pan, T. Wu, B. Zhang, J. Li, T. Yi, Z. Zhang, X. Yang, *Catalysis Science & Technology* **2015**, *5*, 1314-1322; bD. A. K. a. S. S. Soni, *Catal. Sci. Technol.* **2013**, *3*, 469-474.

[5] aH. Wang, C. Zhu, D. Li, Q. Liu, J. Tan, C. Wang, C. Cai, L. Ma, *Renewable and Sustainable Energy Reviews* **2019**, *103*, 227-247; bX. Liu, M. Zhang, Z. Li, *ACS Sustainable Chemistry & Engineering* **2020**, *8*, 4801-4808; cD. Zhang, M.-J. Dumont, *Journal of Polymer Science Part A: Polymer Chemistry* **2017**, *55*, 1478-1492.

[6] aD. Zhao, D. Rodriguez-Padron, K. S. Triantafyllidis, Y. Wang, R. Luque, C. Len, *ACS Sustainable Chemistry & Engineering* **2020**, *8*, 3091-3102; bS. Gajula, K. Inthumathi, S. R. Arumugam, K. Srinivasan, *ACS Sustainable Chemistry & Engineering* **2017**, *5*, 5373-5381.

[7] aO. R. Schade, K. F. Kalz, D. Neukum, W. Kleist, J.-D. Grunwaldt, *Green Chemistry* **2018**, *20*, 3530-3541; bM. Ventura, A. Dibenedetto, M. Aresta, *Inorganica Chimica Acta* **2018**, *470*, 11-21; cZ. Zhang, G. W. Huber, *Chemical Society reviews* **2018**, *47*, 1351-1390.

[8] aS. E. Davis, L. R. Houk, E. C. Tamargo, A. K. Datye, R. J. Davis, *Catalysis Today* **2011**, *160*, 55-60; bX. Pan, S. Wu, D. Yao, L. Liu,

L. Zhang, Z. Yao, Y. Pan, S. Chang, B. Li, *Reaction Chemistry & Engineering* **2020**, *5*, 1397-1404.

[9] M. T. Munekata, G. , *Agric. Biol. Chem* **1981**, 2149-2150.

[10] aA. Brandolese, D. Ragno, G. Di Carmine, T. Bernardi, O. Bortolini, P. P. Giovannini, O. G. Pandoli, A. Altomare, A. Massi, *Organic & biomolecular chemistry* **2018**, *16*, 8955-8964; bJ. D. O. A. C. Braisted, W. L. Delano, J. Hyde,, N. W. R. S. McDowell, C. Yu, M. R. Arkin and, B. C. Raimundo, *J. Am. Chem. Soc* **2003**, *125*, 3714-3715.

[11] A. A. Rosatella, S. P. Simeonov, R. F. M. Frade, C. A. M. Afonso, *Green Chemistry* **2011**, *13*, 754.

[12] F. Wang, Z. Zhang, *Journal of the Taiwan Institute of Chemical Engineers* **2017**, *70*, 1-6.

[13] D. Zhao, D. Rodriguez-Padron, R. Luque, C. Len, *ACS Sustainable Chemistry & Engineering* **2020**, *8*, 8486-8495.

[14] T. Gao, T. Gao, W. Fang, Q. Cao, *Molecular Catalysis* **2017**, *439*, 171-179.

[15] L. Gao, K. Deng, J. Zheng, B. Liu, Z. Zhang, *Chemical Engineering Journal* **2015**, *270*, 444-449.

[16] Z. Zhang, B. Liu, K. Lv, J. Sun, K. Deng, *Green Chemistry* **2014**, *16*, 2762.

[17] F. N. Maria Ventura, Elvira de Giglio,Stefania Cometa, Angela Altomare, Angela Dibenedetto,, *Green Chemistry* **2018**, *20 (17)*, 3921-3926.

[18] M. Ventura, F. Lobefaro, E. de Giglio, M. Distaso, F. Nocito, A. Dibenedetto, *ChemSusChem* **2018**, *11*, 1305-1315.

[19] F. Nocito, M. Ventura, M. Aresta, A. Dibenedetto, *ACS omega* **2018**, *3*, 18724-18729.

[20] aJ. Wang, Y. Wang, W. Wang, T. Peng, J. Liang, P. Li, D. Pan, Q. Fan, W. Wu, *Environmental pollution* **2020**, *262*, 114373; bJ. Xu, X. Qi, C. Luo, J. Qiao, R. Xie, Y. Sun, W. Zhong, Q. Fu, C. Pan, *Nanotechnology* **2017**, *28*, 425701.

[21] N. Ma, Y. Song, F. Han, G .I . N. Waterhouseb, Y. Li, S. Y. Ai, *Catalysis Science & Technology* **2020**, *10*, 4010-4018.

[22] Y. Ma, K. Hu, Y. Sun, K. Iqbal, Z. Bai, C. Wang, X. Jia, W. Ye, *The Science of the total environment* **2019**, *696*, 134013.

[23] D. Ariyanti, L. Mills, J. Dong, Y. Yao, W. Gao, *Materials Chemistry and Physics* **2017**, *199*, 571-576.

[24] aX. He, X. Yi, F. Yin, B. Chen, G. Li, H. Yin, *Journal of Materials Chemistry A* **2019**, *7*, 6753-6765; bP. Sudarsanam, B. Hillary, M. H. Amin, S. B. A. Hamid, S. K. Bhargava, *Applied Catalysis B: Environmental* **2016**, *185*, 213-224.

[25] L. Zhang, L. Li, Y. Cao, X. Yao, C. Ge, F. Gao, Y. Deng, C. Tang, L. Dong, *Applied Catalysis B: Environmental* **2015**, *165*, 589-598.

[26] aL. C. Xiaojiang Yao, Jun Cao, Fumo Yang, Wei Tan, and Lin Dong, *Industrial & Engineering Chemistry Research* **2018**, *57*, 12407-12419; bR. Siavash Moakhar, G. K. L. Goh, A. Dolati, M. Ghorbani, *Applied Catalysis B: Environmental* **2017**, *201*, 411-418.

[27] S. Chen, J. Bi, Y. Zhao, L. Yang, C. Zhang, Y. Ma, Q. Wu, X. Wang, Z. Hu, *Advanced Materials* **2012**, *24*, 5593-5597.

[28] Y. Kang, W. Wang, J. Li, Y. Mi, H. Gong, Z. Lei, *Journal of colloid and interface science* **2020**, *578*, 796-804.

[29] Z. Zhang, D. Gao, D. Xue, Y. Liu, P. Liu, J. Zhang, J. Qian, *Nanotechnology* **2019**, *30*, 395401.

[30] J. C. H. Xu, C. Shan, B. Wang, P. Xi, W. Liu, Y. Tang, *Angew. Chem. Int. Ed* **2018**, *57*, 8654-8658.

[31] aY. Tian, Y. Y. Cao, F. Pang, G. Q. Chen, X. Zhang, *RSC Adv.* **2014**, *4*, 43204-43211; bJ. Wang, J. Bao, Y. Zhou, Y. Zhang, B. Sun, M. Wang, X. Sheng, W. Liu, C. Luo, Y. Xue, C. Guo, X. Chen, *Journal of Solid State Electrochemistry* **2019**, *24*, 137-144.

[32] J. S. Wang, H. M. Ye, Q. H. Qin, J. Xu, X. Q. Feng, *Proceedings of the Royal Society A: Mathematical, Physical and Engineering Sciences* **2011**, *468*, 609-633.

[33] aW. Zhu, X. Tang, F. Gao, H. Yi, R. Zhang, J. Wang, C. Yang, S. Ni, *Chemical Engineering Journal* **2020**, *385*, 123797; bS. Liang, T. Xu, F. Teng, R. Zong, Y. Zhu, *Applied Catalysis B: Environmental* **2010**, *96*, 267-275.

[34] P. F. Zhao, P. F. Yu, Z. J. Feng, Chen R., L. W. Jia, J. Q. Wang, M. Q. Shen, and B. Shan, *RSC Adv* **2016**, *6*, 65950-65959.

[35] Z. Qu, K. Gao, Q. Fu, Y. Qin, *Catalysis Communications* **2014**, *52*, 31-35.

[36] S. Xu, P. Zhou, Z. Zhang, C. Yang, B. Zhang, K. Deng, S. Bottle, H. Zhu, *Journal of the American Chemical Society* **2017**, *139*, 14775-14782.

[37] T. Gao, J. Chen, W. Fang, Q. Cao, W. Su, F. Dumeignil, *Journal of Catalysis* **2018**, *368*, 53-68.

[38] H. Liu, W. Li, M. Zuo, X. Tang, X. Zeng, Y. Sun, T. Lei, H. Fang, T. Li, L. Lin, *Industrial & Engineering Chemistry Research* **2020**, *59*, 4895-4904.

[39] X. Han, C. Li, X. Liu, Q. Xia, Y. Wang, *Green Chemistry* **2017**, *19*, 996-1004.

[40] aV. Makwana, *Journal of Catalysis* **2002**, *210*, 46-52; bS. Mandal, C. Santra, K. K. Bando, O. O. James, S. Maity, D. Mehta, B.

10.1002/cctc.202100091

Chowdhury, *Journal of Molecular Catalysis A: Chemical* **2013**, *378*, 47-56.

10.1002/cctc.202100091

# Entry for the Table of Contents

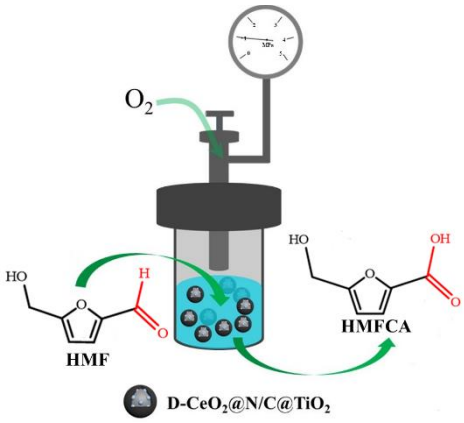


Defective D-$CeO_2$@N/C@$TiO_2$ nanospheres, each comprising a spherical $CeO_2$ core coated with shells of N-doped carbon and $TiO_2$, were successfully synthesized then evaluated for the aerobic oxidation of HMF to HMFCA. Under the optimized reaction conditions (temperature 80 °C, reaction time 30 min, $O_2$ pressure 1 MPa), a high HMF conversion of 87.8% and a remarkable HMFCA selectivity of 100% were obtained, suggesting that the developed noble-metal free catalyst has excellent promise for the synthesis of valuable HMFCA from HMF.